Communication Quality Analysis for WPT and NFC Systems via Broadband Equivalent Circuit Models

Richard Fischbacher, *Graduate Student Member, IEEE*, Jose Romero Lopera, *Member, IEEE*, David Pommerenke, *Fellow, IEEE*, Ralph Prestros, *Member, IEEE*, Bernhard Auinger, *Member, IEEE*, Wolfgang Bösch, *Fellow, IEEE*, and Jasmin Grosinger, *Senior Member, IEEE*

***Abstract*—This letter presents a novel full-system communication quality analysis of a wireless power transfer (WPT) and near-field communication (NFC) system. The analysis is conducted via a thoroughly verified broadband equivalent circuit (EC) model of a WPT and NFC system prototype. Such an EC model can accelerate the iterative system design process for systems with interoperating or coexisting WPT and NFC interfaces. The EC model is verified by measurements of a prototype. EC model and measurements agree excellently by comparing impedance parameters, single-sided frequency spectra, and the signal constellation diagram of the NFC tag-to-reader communication signal. The NFC communication quality analysis shows a severe impairment of the NFC tag-to-reader communication by the WPT system.**

***Index Terms*—Coils, near-field communication (NFC), wireless power transfer (WPT).**

I. Introduction

HANDHELD devices are being equipped with more wireless features, which are forced to coexist and interoperate nearby each other, e.g., wireless charging and mobile payments in smartphones or smartwatches [1], [2]. For wireless charging, handheld devices typically use specific wireless power transfer (WPT) standards, e.g., the Qi standard [3], which transmits energy via magnetic resonant coupled devices at roughly 100 kHz. Mobile payments are typically realized via near-field communication (NFC), which transmits data via magnetic resonant coupled devices at 13.56 MHz [4]. WPT and NFC systems integrated into chargers (transmitter, TX) and handheld devices (receiver, RX) might impair each other's functionalities when coexisting or interoperating [5].

Recent work on WPT and NFC systems coexistence and interoperability is given in Table I. Researchers have been investigating coexisting WPT and NFC systems via inductive decoupling using novel coil shapes [6] and coil positioning [7] to reduce the inductive coupling between WPT and NFC coils. Further work used frequency separation techniques to enable interoperating WPT and communication systems. Here, researchers realized a WiFi communication link for WPT [8], [9], and NFC at higher frequencies [10]. In this letter, we investigate the coexistence of WPT and NFC systems. In contrast to previous work, we present a solution that allows us to analyze the NFC system communication quality directly to improve the coexistence and interoperability of WPT and NFC systems.

In previous work [6], [7], [8], [9], [10], researchers used electromagnetic (EM) simulation, measurements, and narrowband equivalent circuit (EC) models [5] to investigate the above-mentioned solutions directly. Contrary to this, we use EM simulations and measurements to generate and verify a novel broadband EC model of a WPT and NFC systems prototype. This broadband EC model allows the investigation of high-order WPT harmonics, contrary to narrowband EC models. In our previous work [11], we presented the basics of physical broadband EC models for two coupled NFC coils and a behavioral EC model for a WPT coil [12]. In this letter, we further expand on this research and combine physical and behavioral coil EC models to generate a WPT and NFC systems prototype EC model. Further, we use this broadband EC model to conduct the NFC system communication quality analysis. The use of an EC model has all advantages of circuit-level simulation tools [13] and can be used for a fast and efficient iterative system design process.

II. Broadband EC Model

Fig. 1(a) shows the WPT and NFC system prototype used in this work, consisting of a WPT TX, WPT RX, NFC reader, and NFC tag. The WPT system coexists and interferes with an active NFC system. The TX and RX coils are aligned in a coaxial and coplanar manner with the coil distances being $d_1 = 15$ mm and $d_2 = 3$ mm. The four subsystems are realized with a coil printed circuit board (PCB) [see Fig. 1(b)] and its respective tuning circuit PCB [see Figs. 1(a) and 3]. The WPT TX and RX coils were provided by Würth Elektronik [14] and the tuning circuits were custom-built. Both are in accordance with the Qi standard [3]. The NFC reader and tag coils were custom-built (NFC class 5 form factor [15]) and the tuning circuits are based on state-of-the-art designs [16].

The EC models of the coupled coils are based on our previous work and are shown in Fig. 2 [11]. The chosen frequency range of interest is 0.1–60 MHz. We advanced a standard coil EC model ($L_{\mathrm{n,r/t,i}}$, $R_{\mathrm{n,r/t,i}}$, $R_{\mathrm{p,n,r/t,1}}$, and $C_{\mathrm{p,n,r/t,1}}$) [11], [17] for the coupled NFC coils while spreading the coupling capacitances C_{c}

Manuscript received 1 August 2023; accepted 27 August 2023. Date of publication 11 September 2023; date of current version 5 January 2024. This work was supported by the "University SAL Labs" initiative of Silicon Austria Labs (SAL) and its Austrian partner universities for applied fundamental research for electronic-based systems. *(Corresponding author: Richard Fischbacher.)*

Richard Fischbacher, Jose Romero Lopera, and David Pommerenke are with the Graz University of Technology, 8010 Graz, Austria, and also with the Silicon Austria Labs, 8010 Graz, Austria (e-mail: richard.fischbacher@tugraz.at; romerolopera@tugraz.at; david.pommerenke@tugraz.at).

Ralph Prestros and Bernhard Auinger are with the Silicon Austria Labs, 8010 Graz, Austria (e-mail: ralph.prestros@silicon-austria.com; bernhard.auinger@silicon-austria.com).

Wolfgang Bösch and Jasmin Grosinger are with the Graz University of Technology, 8010 Graz, Austria (e-mail: wbosch@tugraz.at; jasmin.grosinger@tugraz.at).

Digital Object Identifier 10.1109/LAWP.2023.3314198

TABLE I
RELATED WORK OF WPT COEXISTENCE AND INTEROPERABILITY INVESTIGATIONS

References	Inductive WPT system		Communication system		Solution / Methodology
	Frequency	Coil	Type	Antenna	
[6]	110 kHz	Planar square 50 mm	NFC (13.56 MHz)	Planar square 50 mm	Inductive decoupling via coil shape design / EM simulation
[7]	6.78 MHz	Varying shapes	NFC (13.56 MHz)	Planar rectangular 117 mm x 62 mm	Inductive decoupling via coil positioning / EM simulation and measurement
[8], [9]	100 kHz	Planar square	WiFi protocol (5.24 GHz)	Patch antenna 12 mm	Frequency separation / EM simulation, measurement, and narrowband EC model
[10]	12 MHz	Circular 36 mm radius	Inductive coupling at 90 MHz and 135 MHz	Circular 36 mm radius	Frequency separation / Measurement and narrowband EC model
This work	106 kHz	Planar circular 25 mm radius [14]	NFC (13.56 MHz)	Planar circular 17.5 mm radius	Communication quality analysis / EM simulation, measurement, and broadband EC model

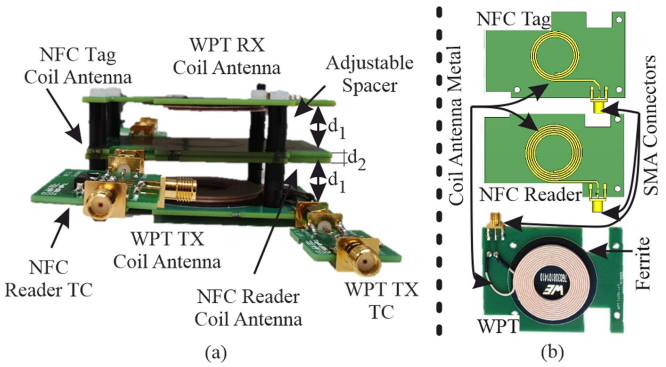

Fig. 1. WPT and NFC prototype setup including coils and tuning circuits: The prototype is shown in (a) and the separate coils are shown in (b) [11].

over the inductance and DC resistance [11]. The WPT coil was modeled using a behavioral modeling approach [12] with parallel resonant circuits ($L_{\mathrm{w,rx/tx,i}}$, $R_{\mathrm{w,rx/tx,i}}$, $R_{\mathrm{p,w,rx/tx,i}}$, and $C_{\mathrm{p,w,rx/tx,i}}$) to align the EC model behavior with the measured prototype behavior [11]. In this specific case, the chosen frequency range and used WPT coils dictate the use of three resonant circuits for the WPT coil EC models [11], which in turn requires the NFC coil inductance to be split into three parts ($i = 1, 2, 3$, Fig. 2). The coils interact with one another by inductive and capacitive coupling, which are implemented in the EC model using coupling coefficients k and coupling capacitances C_{c}.

The tuning circuits of the coupled coils are shown in Fig. 3. The WPT TX and NFC reader circuits are either connected to a vector network analyzer (VNA, R&S ZVL) or a 50 Ω arbitrary waveform generator (AWG, Keysight 33600 A) for system analysis. The WPT tuning circuits are discussed in [5]. The NFC reader tuning circuit topology is given in [16]. It uses an inductance (modeled via a coil standard EC model $R_{\mathrm{n,r,f}}$, $C_{\mathrm{n,r,p,f}}$, $R_{\mathrm{n,r,p,f}}$, and $L_{\mathrm{n,r,f}}$) and the capacitance $C_{\mathrm{n,r,f}}$ as a low-pass filter, the capacitances $C_{\mathrm{n,r,1/2}}$ to set the series resonance frequency of the NFC reader to 13.56 MHz (while only being coupled with the NFC tag), and the resistance $R_{\mathrm{n,r}}$ to adjust the quality factor. Usually, one would design a parallel resonance, but it is not required for EC model verification purposes. In addition, we added the resistance $R_{\mathrm{n,a}}$ to adjust the input impedance at port NFC (see Fig. 3) at 13.56 MHz, to align the quality factor between measurement and simulation. The NFC tag tuning circuit uses the resistance $R_{\mathrm{n,t}}$ to set the quality factor, the capacitance $C_{\mathrm{n,t}}$ as combined tag chip and tuning capacitance to set the resonance frequency of the NFC tag to 13.56 MHz, and the resistance $R_{\mathrm{n,chip}}$ to model the tag chip resistance [18]. The load modulation switch (LM Switch) is realized via two transistors [19], [20].

III. EC MODEL VERIFICATION

Vector network analyzer measurements are required to determine scattering (S) and impedance (Z) parameters of the single coils and prototype [11]. Each coil was measured with no other coils in close proximity to determine the lumped elements for the single-coil EC models. These measurement results need to be adjusted for the prototype coil arrangement shown in Fig. 1(a), due to the WPT ferrites. The inductance of each coil has to be re-evaluated by conducting one port measurements of each coil while being assembled in the prototype coil arrangement (without tuning circuits). The DC resistances were not adjusted. The introduced loss of the ferrite and other material might be the cause why $R_{\mathrm{n,a}}$ is required to adjust the magnitude at 13.56 MHz.

We determine the coupling coefficients between the coils via a two-port measurement [11], where each port of the VNA is connected to a coil. The resulting transmission impedance parameter Z_{12} between two coils is used to calculate the mutual inductance $M = \mathrm{Im}\{Z_{12}\}/\omega$ and the coupling coefficient $k = M/\sqrt{L_1 \cdot L_2}$, where ω is the angular frequency and $L_{1/2}$ are the coil inductances. It is important to conduct these measurements within the prototype setup (without tuning circuits) while the not measured coils are terminated with an open circuit. The coupling capacitances C_{c} are determined by connecting each Balun output to a coil, forming a capacitance via the two coils, represented by the imaginary part of its Z-parameter (Z_{11}). The capacitance is then calculated via $C_{\mathrm{c}} = -1/(\omega \cdot \mathrm{Im}\{Z_{11}\})$ [11]. In contrast to previous work [11] due to the coupling of behavioral and physical EC models, we did not split the inductances $L_{\mathrm{n,r/t,i}}$, resistances $R_{\mathrm{n,r/t,i}}$, and coupling capacitances $C_{\mathrm{c,1..6,i}}$ evenly. We divide them according to the inductance ratios of the WPT coil inductances. The values are given in the Fig. 2 description, leading to the overall best EC model and prototype impedance parameter agreement. Fig. 4 shows the impedance parameter magnitude of the prototype with port 1 being connected to port WPT and port 2 being connected to port NFC (see Fig. 3). It compares measurement ($|Z_{11}|$ M, $|Z_{12}|$ M, and $|Z_{22}|$ M), EC model ($|Z_{11}|$ EC, $|Z_{12}|$ EC, and $|Z_{22}|$ EC), and EM simulation

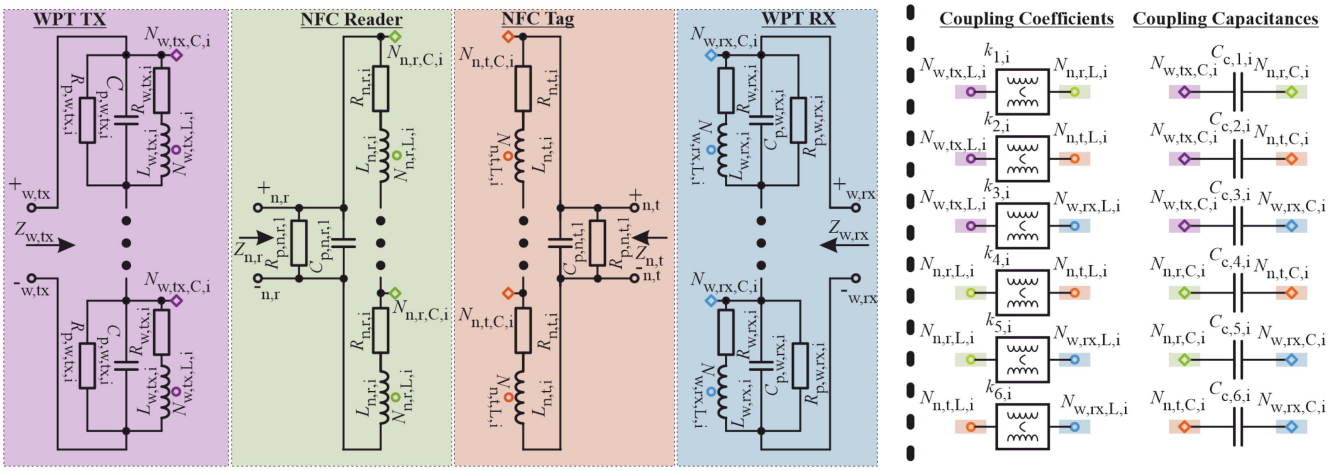

Fig. 2. EC coil and coil coupling models: Lumped element values for the left-hand side figure are given in Table II. Coupling coefficients k and coupling capacitances C_c connect two inductances or circuit nodes depending on the node names N: $k_{1,i} = 0.223$, $C_{\mathrm{c},1,i} = [1.99, 0.014, 0.059]$ pF, $k_{2,i} = 0.128$, $C_{\mathrm{c},2,i} = [1.35, 0.001, 0.041]$ pF, $k_{3,i} = 0.075$, $C_{\mathrm{c},3,i} = [1.45, 0.011, 0.044]$ pF, $k_{4,i} = 0.455$, $C_{\mathrm{c},4,i} = [6.14, 0.045, 0.185]$ pF, $k_{5,i} = 0.155$, $C_{\mathrm{c},5,i} = [1.86, 0.013, 0.055]$ pF, $k_{6,i} = 0.182$, and $C_{\mathrm{c},6,i} = [1.69, 0.012, 0.051]$ pF for $i = 1, 2, 3$. The $+$ and $-$ nodes indicate the nodal connections with the tuning circuits in Fig. 3. Colors indicate the associated coil EC model, tuning circuits, and coupling elements.

TABLE II
COIL LUMPED ELEMENT VALUES FOR THE EC MODEL SHOWN IN FIG. 2

/ $i =$	$L_{i,1}$ μH	$L_{i,2}$ nH	$L_{i,3}$ nH	$R_{i,1}$ mΩ	$R_{i,2}$ mΩ	$R_{i,3}$ mΩ	$R_{\mathrm{P},i,1}$ kΩ	$R_{\mathrm{P},i,2}$ Ω	$R_{\mathrm{P},i,3}$ Ω	$C_{\mathrm{P},i,1}$ pF	$C_{\mathrm{P},i,2}$ pF	$C_{\mathrm{P},i,3}$ pF
w,tx and w,rx	21.99	159	661	116	0.1	3.3	11.8	314	807	31.3	23.5	34.2
n,r	0.998	7.2	30	212	1.5	6.4	43.4	/	/	3.9	/	/
n,t	0.405	2.9	12.2	106	0.8	3.2	31.3	/	/	3.6	/	/

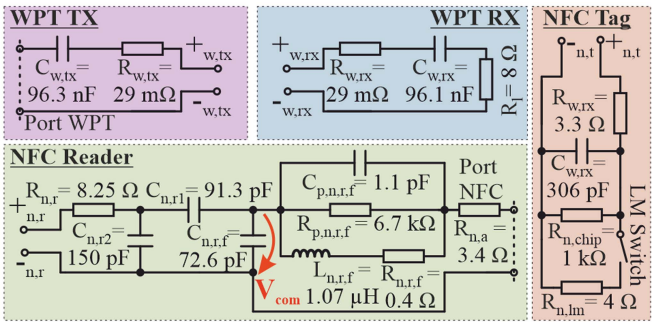

Fig. 3. Tuning circuits EC models: It shows the actual schematics except for $R_{\mathrm{n,a}}$ and the filter inductance EC model. The $+$ and $-$ nodes indicate the nodal connections with the tuning circuits shown in Fig. 2.

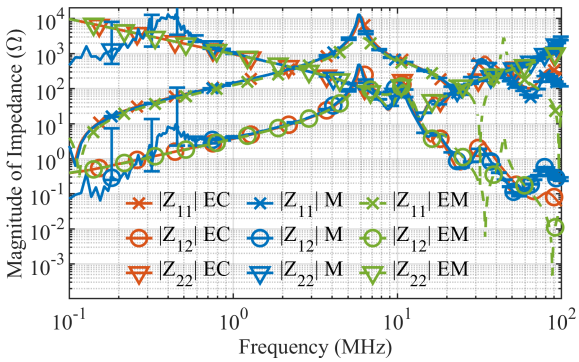

Fig. 4. Magnitude of the impedance parameters Z_{11}, Z_{12}, and Z_{22} of the prototype: Measurement results show mean values of 100 measurement runs, including minimum and maximum values with error bars.

($|Z_{11}|$ EM, $|Z_{12}|$ EM, and $|Z_{22}|$ EM). The prototype coil stack was modeled in CST [21], and its S-parameters were extracted and applied to the same tuning circuits as used in the EC model. We used annealed copper for metals, FR-4 for PCBs, and modeled the ferrite according to its datasheet. The EC model and measurement results agree very well between 1 and 60 MHz. $|Z_{12}|$ M and $|Z_{22}|$ M show measurement inaccuracies below 1 MHz due to dynamic range issues caused by the measurement devices. The upper-frequency limit of 60 MHz could be raised by introducing more WPT coil parallel resonant circuits (see Fig. 2). We chose three as a compromise between bandwidth and EC model complexity. The EM simulation agrees with the EC models below 1 MHz and shows good agreement with measurements up to 20 MHz, but at higher frequencies uncertainties are caused by material parameters [22] and simplifications of the 3-D model.

IV. COMMUNICATION QUALITY ANALYSIS

Further, the EC model is verified by comparing the NFC tag-to-reader communication to evaluate how well the EC model can be used to conduct NFC communication quality analysis.

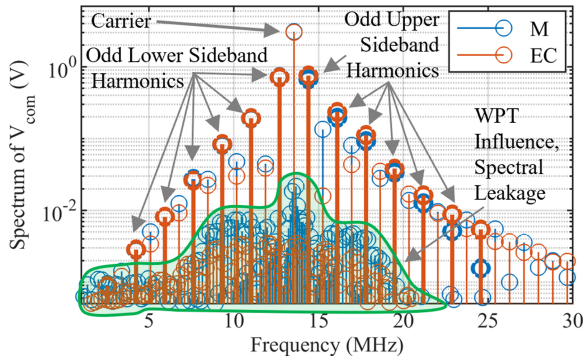

Fig. 5. Single-sided frequency spectrum of V_{com} (see Fig. 3): The different components of the V_{com} spectrum (lower sideband, upper sideband, WPT harmonics, noise, and carrier) are illustrated.

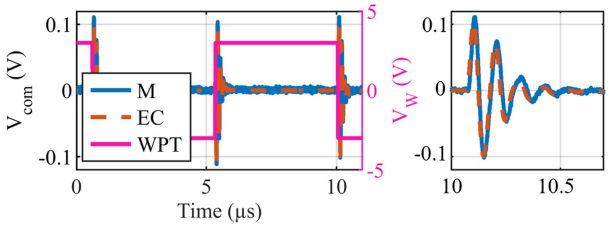

Fig. 6. WPT signal at NFC reader: The signal V_{com} is shown while only the WPT source is active (i.e., NFC reader source is not active and replaced by a 50 Ω resistance). The right-hand figure has a zoomed-in x-axis to show how well the measurement and EC model waveforms agree.

Here, we supply square waves $V_{w,pp} = 6$ V with 105.9375 kHz to port WPT and $V_{n,pp} = 4$ V with 13.56 MHz to port NFC by two 50 Ω sources of the AWG via a coaxial cable and Balun [23]. In addition, the LM switch is actuated with $2 \cdot 847.5$ kHz to carry out LM with 847.5 kHz [15], [24]. The NFC tag-to-reader communication signal V_{com} is usually determined, as shown in Fig. 3. We determine this signal in measurement via an oscilloscope (R&S RTO 2044) and a differential probe (R&S ZD-30) and in circuit-level simulation using the previously described EC model. This EC model includes S-parameter descriptions of the cables and Baluns to include their behavior in the simulations.

The single-sided frequency spectrum of the measured (M) and simulated (EC) V_{com} time signal is calculated via a fast Fourier transform (FFT) and shown in Fig. 5. The chosen FFT boundary conditions lead to frequency bins at integer multiples of the WPT square wave frequency. The figure shows the NFC carrier, odd upper and lower sideband harmonics, and WPT signal versus frequency. The upper and lower sidebands are NFC tag-to-reader communication signals caused by LM. These show excellent agreement between measurement and simulation for the lower sideband and slight errors at the upper sidebands. Since the WPT harmonics are difficult to compare while the NFC source is active (spectral leakage and limited oscilloscope resolution), we show measured and simulated V_{com} in Fig. 6, with only the WPT source being active. The figure shows excellent agreement between measurement and simulation, verifying that the EC model accurately describes the WPT TX and NFC reader interaction.

In addition, we conduct ideal in-phase/quadrature-phase (I/Q) demodulation of the communication signal V_{com} [25]. The corresponding signal constellation diagram is shown in Fig. 7, showing mean values and the accompanying error bars for the logical states "0" and "1." Measurement and simulation show excellent agreement (EC and M, see Fig. 7). Realistic WPT and NFC systems would use different source impedances and might have to use different tuning setups when tuning the NFC reader with a strongly coupled (SC) tag in mind.

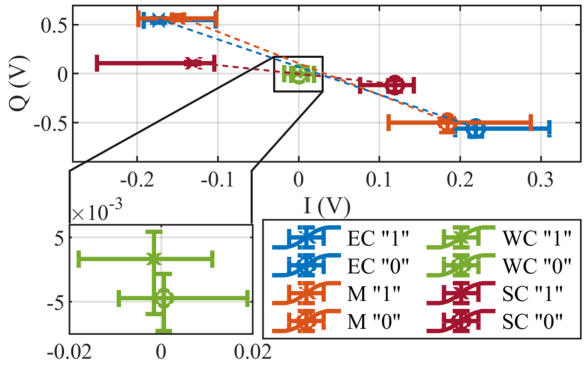

Fig. 7. Signal constellation diagram: The signal V_{com} is I/Q demodulated and separated into logical states "0" and "1."

Further, we conducted a WPT and NFC systems coexistence analysis for a SC (3 mm NFC coil distance, $k_{4,i} = 0.455$, and $C_{c,4,i} = [6.14, 0.045, 0.185]$ pF for $i = 1, 2, 3$) and weakly coupled (WC, 15 mm NFC coil distance, $k_{4,i} = 0.098$, and $C_{c,4,i} = [0.84, 0.006, 0.025]$ pF for $i = 1, 2, 3$) NFC coils, while keeping all other coupling interactions constant (see Fig. 2). As a first step, we adjusted the NFC reader tuning circuit via $L_{n,r,f} = 107$ nH, $C_{n,r,f} = 590$ pF, $C_{n,r1} = 820$ pF, and $C_{n,r2}$ being replaced by the inductance $L_{n,r2} = 350$ nH, resulting in an NFC tuning setup with a parallel resonance of the NFC reader at 15 MHz, while being SC to the NFC tag. In addition, we adjusted the inner resistance of the WPT source (0.8 Ω) and the NFC source (5 Ω). The SC results show a significant distance between the logical "0" and "1" states (see Fig. 7). Detuning the system by applying a WC interaction between NFC coils leads to a significant overlap of logical states, indicating possible issues regarding the NFC communication quality. The main reason is the signal created by the WPT source during switching operations (see Fig. 6).

V. Conclusion

We generated a broadband EC model to investigate the coexistence of WPT and NFC systems. VNA measurements verify the EC model, showing an excellent agreement of the impedance parameters in the frequency range from 1 to 60 MHz. NFC tag-to-reader communication shows an excellent agreement for measurement and EC model. Further, we investigated how NFC tag-to-reader communication could be impaired by WPT via a signal constellation diagram. In addition, the misalignment of RX and TX has to be investigated. Coil misalignment leads to a change in the coupling coefficient [26], which can be easily modeled by the presented solution [4]. However, misalignments will also lead to a change in capacitive coupling between the close-by coils. Future work has to focus on calculating capacitive coupling between the coils for a specific misalignment, which can then be modeled in the presented solution.

REFERENCES

[1] NXP Semiconductors"Mobile products," 2023. Accessed: Sep. 1, 2023. [Online], Available: https://bit.ly/2DjlLIz

[2] M. Rajabi, N. Pan, S. Claessens, S. Pollin, and D. Schreurs, "Modulation techniques for simultaneous wireless information and power transfer with an integrated rectifier–receiver," *IEEE Trans. Microw. Theory Techn.*, vol. 66, pp. 2373–2385, May 2018.

[3] "The Qi Wireless Power Transfer System Power Class 0 Specification," Wireless Power Consortium, Version 1.2.3, Feb. 2017.

[4] J. Grosinger, "Robustly operating: Passive near-field communication systems in metal environments," *IEEE Microw. Mag.*, vol. 24, no. 4, pp. 30–39, Apr. 2023.

[5] R. Fischbacher et al., "EC model for WPT and NFC systems interoperability analysis," in *Proc. IEEE Radio Wireless Symp.*, 2021, pp. 112–115.

[6] S. Hong et al., "Dual-directional near field communication tag antenna with effective magnetic field isolation from wireless power transfer system," in *Proc. IEEE Wireless Power Transfer Conf.*, 2017, pp. 1–3.

[7] M. Kang, E. Noh, and K. Kim, "NFC transmitter coil placement to minimise degradation of A4WP wireless power transfer efficiency," *Electron. Lett.*, vol. 53, pp. 616–618, Mar. 2017.

[8] A. Pacini, F. Berra, D. Masotti, and A. Costanzo, "Uniform sliding system for simultaneous WPT and communication data transfer," in *Proc. IEEE Radio Wireless Symp.*, 2019, pp. 1–3.

[9] A. Pacini, "Design of novel systems for position independent energy and data transfer," Ph.D. dissertation, Univ. Bologna, Bologna, Italy, Apr. 2019.

[10] M. Dionigi and M. Mongiardo, "Multi band resonators for wireless power transfer and near field nagnetic communications," in *Proc. IEEE MTT-S Int. Microw. Workshop Ser. Innov. Wireless Power Transmiss. Technol., Syst., Appl.*, 2012, pp. 61–64.

[11] R. Fischbacher, D. Pommerenke, R. Prestros, J. R. Lopera, W. Bösch, and J. Grosinger, "Broadband EC models of coil antennas for inductively coupled systems," in *Proc. IEEE Wireless Power Week*, 2022, pp. 465–469.

[12] J. C. Pedro and S. A. Maas, "A comparative overview of microwave and wireless power-amplifier behavioral modeling approaches," *IEEE Trans. Microw. Theory Techn.*, vol. 53, no. 4, pp. 1150–1163, Apr. 2005.

[13] F. Berra, A. Costanzo, J. Grosinger, and L. Görtschacher, "Space mapping design method for an antenna transducer of a bend sensor RFID tag," in *Proc. 47th Eur. Microw. Conf.*, 2017, pp. 109–112.

[14] Würth Elektronik, "WE-WPCC wireless power transfer transmitter coil - 760308101410," 2019. [Online]. Available: https://bit.ly/3sTOJse

[15] "Identification cards–Contactless integrated circuit cards – Proximity cards," ISO/IEC 14443, 2018.

[16] "NXP Semiconductors"PN7120 antenna design and matching guide," 2016. Accessed: Sep. 1, 2023. [Online]. Available: https://bit.ly/2CdlIgL

[17] T. Bauernfeind, W. Renhard, S. Schmethanner, M. Gebhard, and K. Preis, "Equivalent circuit parameter extraction for controlled detuned NFC antenna systems utilizing thin ferrite foils," in *Proc. 12th Int. Conf. Telecommun.*, 2013, pp. 251–256.

[18] J. Grosinger, B. Deutschmann, L. Zöscher, M. Gadringer, and F. Amtmann, "HF RFID tag chip impedance measurements," *IEEE Trans. Instrum. Meas.*, vol. 71, Nov. 2021, Art. no. 2000911.

[19] STMicroelectronics, "RF power transistor PD85004," 2008. [Online]. Available: https://bit.ly/3PljUnN

[20] Infineon, "Safe and reliable MOSFET operation in bidirectional power switch (BDPS) applications," 2021. Accessed: Sep. 1, 2023. [Online]. Available: https://bit.ly/3JNgkS4

[21] Dassault Systémes, "CST Studio Suite," 2023. [Online]. Available: http://bit.ly/3Rp0Vvb

[22] R. Fischbacher et al., "On the difficulties to determine the intrinsic material parameters for MnZn ferrites," in *Proc. Int. Symp. Exhib. Electromagn. Compat.*, 2023.

[23] Coilcraft, "Datasheet of Balun PWB3010LC," 2017. [Online]. Available: https://bit.ly/3LlOWLi

[24] "ISO/IEC 18092 Information Technology – Telecommunications and Information Exchange between Systems – Near Field Communication – Interface and Protocol," ISO/IEC 18092.

[25] J. Finol and M. Buchholz, "Design of an inphase and quadrature phase and amplitude imbalance compensation in quadrature receivers," in *Proc. IEEE 5th Int. Caracas Conf. Devices*, Circuits and Systems, Punta Cana, Dominican Republic, 2005, pp. 254–258.

[26] J. R. Lopera, R. Fischbacher, D. Pommerenke, R. Prestros, B. Auinger, and J. Grosinger, "Adaptive NFC WPT system implementing neural network-based impedance matching with bypass functionality," in *Proc. Int. Microw. Symp.*, 2023, pp. 879–882.